Soft synthesis and vacuum ultraviolet spectra of YAG:Ce^{3+} nanocrystals: reassignment of Ce^{3+} energy levels

2007 J. Phys.: Condens. Matter 19 216213

(http://iopscience.iop.org/0953-8984/19/21/216213)

IOP PUBLISHING JOURNAL OF PHYSICS: CONDENSED MATTER

J. Phys.: Condens. Matter **19** (2007) 216213 (14pp) doi:10.1088/0953-8984/19/21/216213

Soft synthesis and vacuum ultraviolet spectra of YAG:Ce^{3+} nanocrystals: reassignment of Ce^{3+} energy levels

Peter A Tanner[1], Lianshe Fu[1], Lixin Ning[2], Bing-Ming Cheng[3] and Mikhail G Brik[4]

[1] Department of Biology and Chemistry, City University of Hong Kong, Tat Chee Avenue, Kowloon, Hong Kong SAR, People's Republic of China
[2] Universita di Milano-Bicocca, Dipartimento di Scienza dei Materiali, via Cozzi 53, 20125 Milano, Italy
[3] National Synchrotron Radiation Research Center, 101 Hsin-Ann Road, Hsinchu Science Park, Hsinchu 30076, Taiwan, Republic of China
[4] Fukui Institute for Fundamental Chemistry, Kyoto University, Takano, Sakyo, Kyoto 606-8103, Japan

Received 22 December 2006, in final form 4 April 2007
Published 27 April 2007
Online at stacks.iop.org/JPhysCM/19/216213

Abstract

Ce^{3+}-doped YAG nanoparticles have been synthesized at relatively low temperatures by the co-precipitation and polymer-assisted sol–gel methods and characterized by Fourier transform infrared spectroscopy (FT-IR), x-ray diffraction (XRD) and x-ray absorption near-edge structure (XANES) measurements. Calcination of the product was carried out at temperatures between 800 and 1100 °C. Products calcined at the lower temperature contained a greater proportion of Ce^{4+}, and this contributed in part to the lower intensity of the characteristic yellow photoluminescence. The synchrotron radiation excitation spectrum of this yellow emission band exhibits bands due to Ce^{3+} absorption as well as the host band gap. The origin of a luminescence band at about 300 nm obtained under band-gap excitation is discussed. Previous assignments of the 5d electronic energies in YAG:Ce^{3+} are critically assessed, and in the light of the new energy level and transition intensity calculations a revised assignment is put forward for the 5d energy levels.

(Some figures in this article are in colour only in the electronic version)

1. Introduction

Yttrium aluminium garnet ($Y_3Al_5O_{12}$, YAG) doped with Ce^{3+} (YAG:Ce^{3+}) is an important material because as well as its scintillation properties [1, 2] it can efficiently convert the blue light-emitting diode radiation into a very broad yellow emission band [3, 4]. This material is conventionally synthesized by a high-temperature solid-state reaction of Al_2O_3 and Y_2O_3

Table 1. Literature data for band maxima in the electronic spectra of YAG:Ce^{3+}. The energies are expressed in cm^{-1} (and are not rounded to the appropriate precision).

Temp.	Band energy (cm^{-1})							Ref[a]
RT			43 478		29 412		21 739	[1] A[b]
RT			44 444		28 986		22 222	[4] E
RT			44 843		29 412	26 882	21 739	[5] A
RT			∼45 600	∼39 090	29 412		21 739	[16] A
78 K		48 877	44 401	38 311	29 439		21 858	[17] A
2 K			43 917	37 736	29 674		21 810	[18] MCD
RT			44 000	37 000	29 400		22 000	[19] A
RT–12 K	53 191		45 045	(37 735)[c]	29 411		21 834	[20] A, E
Mean values		48 877	44 466	38 034	29 393		21 868	

[a] A: absorption spectrum; E: excitation spectrum; MCD: magnetic circular dichroism spectrum.
[b] Ceramic samples.
[c] Absent from the excitation and absorption spectra but assigned by reference to other studies.

near 1600 °C [5], usually resulting in another two intermediate phases: $YAlO_3$ (YAP) and $Y_4Al_2O_9$ (YAM) with large particle sizes. Some samples show OH stretching bands in the infrared absorption spectra [6]. In order to obtain the pure phase at lower temperature and with smaller particle size, wet chemical methods such as sol–gel synthesis, the combustion method and the co-precipitation method have been extensively applied [7–15]. In this work, two synthetic methods were employed, the co-precipitation method and the polymer-assisted sol–gel process, to synthesize YAG:Ce^{3+} nanoparticles, and following its characterization the spectroscopic properties were investigated.

A further aim of the present study was to understand the 5d electron energy level diagram of Ce^{3+} in YAG, which has attracted much discussion in the past several decades. We aimed to do this by rationalizing the excitation and absorption spectra of YAG:Ce^{3+}. The D_2 site symmetry of the Ce^{3+} ion which substitutes for Y^{3+} in the YAG crystal splits the 5d excited state ^2D into five crystal-field levels. The excitation and absorption spectra of YAG:Ce^{3+} have been reported in many studies and the peak maxima, which depend to some extent upon temperature and the concentration of Ce^{3+}, as well as the preparation method [15], are summarized in table 1. All studies are in agreement concerning the location of three of the 4f–5d bands at about 460, 340 and 220 nm, although there are differences in the assignments of the remaining two bands. The most careful and thorough study is that of Tomiki *et al* [17]. The band at 372 nm (26 880 cm^{-1}) observed in [5] was not apparent in other absorption spectra. The band at 261 nm (∼38 000 cm^{-1}) was not observed in some other excitation and absorption spectra, and a lattice defect band in the absorption spectrum of YAG has been reported at 270 nm which is absent in ceramic samples of YAG:Ce^{3+} [1]. The band reported at 188 nm (53 190 cm^{-1}) in [20] more likely corresponds to the bandgap of YAG [21]. The room-temperature emission spectrum of YAG:Ce^{3+} (0.005 at.%) exhibits an intense yellow band at 525 nm which shifts to longer wavelength at 530 nm on increasing the Ce^{3+} dopant ion concentration to 0.5 at.% [1, 22]. In order to rationalize the energy level assignments, energy level and transition intensity calculations are presented in sections 3.1 and 3.2. Together with the literature survey and our synchrotron excitation spectra, the calculations enable energy level assignments to be proposed in section 3.8 which are in agreement with experiment.

2. Experiment

The typical procedure for the synthesis of YAG:0.33% Ce^{3+} using the co-precipitation method was as follows. A total volume of 150 cm^3 aqueous solution containing 18.0 mmol of

$Y(NO_3)_3$, 30.1 mmol of $Al(NO_3)_3{\cdot}9H_2O$ and 0.06 mmol of $Ce(NO_3)_3{\cdot}6H_2O$ with a molar ratio of Y:Al:O:Ce = 2.99:5:12:0.01 (YAG:0.33% Ce^{3+}) was prepared. To the above mixture, 12.6496 g of NH_4HCO_3 (0.16 mmol) in 150 cm^3 of water was added dropwise and a precipitate was formed. The solution containing the precipitate was further stirred for about 10 min and then it was filtered. The precipitate was washed with water and dried at 100 °C overnight. The resultant powders were calcined at 800, 900, 1000 and 1100 °C for 2 h, respectively. The resulting samples were designated as YAG:Ce-C-T (C stands for the co-precipitation method, and T indicates the calcination temperature).

The synthesis of YAG: Ce^{3+} using a polymer-assisted sol–gel process followed the literature procedure [7]. To a 500 cm^3 mixture solution containing 0.0598 M Y^{3+}, 0.0002 M Ce^{3+} and 0.1 M Al^{3+} with a molar ratio of Y:Al:O:Ce = 2.99:5:12:0.01 (YAG:0.33% Ce^{3+}), 30 g of citric acid, 30 g of acrylamide and 10 g of N,N'-methylene-bis-acrylamide were added. Finally, 10 mg of $(NH_4)_2S_2O_8$ were added to initiate the polymerization reaction. By heating the solution at 80 °C, a white gel was formed which was dried at 100 °C overnight. A slow heating process was employed for calcination. The sample was first ground into a powder and heated from 100 to 600 °C at a rate of 2 °C min^{-1}, and kept at that temperature for around 2 h. Then the sample was ground into a powder again and calcined at 800 °C for 4 h. Finally, the sample was divided into several parts and calcined at 900, 1000, and 1100 °C for 2 h, respectively. The resultant samples were designated as YAG:Ce-P-T (P stands for the polymer-assisted sol–gel process, and T as above).

Powder x-ray diffraction (XRD) patterns for all samples were obtained on a Siemens D500 x-ray diffractometer using Cu Kα radiation (λ = 1.54 Å) at 40 kV and 30 mA with a scanning rate of 0.05° s^{-1} in the 2θ range of 15°–75°. FT-IR spectra were measured in the region of 4000–400 cm^{-1} by the KBr pellet technique using a Nicolet Avatar 360 FT-IR spectrophotometer with a resolution of 4 cm^{-1} and employing 16 scans. Continuous wave excitation and emission spectra were recorded on SPEX FluoroMax-3 spectrofluorometer with a 450 W xenon lamp as the excitation source at room temperature. Low-temperature (10 K) emission spectra were recorded at a resolution of 2–4 cm^{-1} using an optical parametric oscillator (Panther) pumped by the third harmonic of a Surelite Nd:YAG pulsed laser. The emission was passed into an Acton 0.5 m monochromator having a 1200 grooves/mm grating blazed at 500 nm and a back-illuminated SpectruMM CCD detector. The sample was housed in an Oxford Instruments closed-cycle cryostat. Excitation and emission spectra were also recorded at a resolution of 0.3–2.5 nm from room temperature down to 10 K using the photoluminescence end station coupled to the high-flux BL03A synchrotron radiation beam line at the National Synchrotron Radiation Center, Hsinchu, Taiwan [23]. Ce L_3 NEXAFS measurements were carried out at BL01B1 in the SPring8, Harima, Japan. The total fluorescence yield (TFY) mode using the 19-element Ge solid-state detector was chosen. The x-rays were monochromatized by a Si(111) double-crystal monochrometer.

3. Results and discussion

3.1. Calculation of 4f and 5d energy levels of Ce^{3+} in YAG

The YAG crystal has a bcc structure (space group $Ia3d$, O_h^{10}, Z = 160) [24]. The large Ce^{3+} ion occupies the 24(c) sites of Y^{3+} with D_2 point group symmetry, and each of the ions is dodecahedrally coordinated to eight O; in garnets medium sized ions, Al^{3+} (VI), occupy octahedral sites (site symmetry C_{3i}) and relatively small ions, Al^{3+} (IV), occupy tetrahedral sites (site symmetry S_4). The crystal-field parameters B_q^k for the D_2 point symmetry relevant in the energy level calculations are those with k = 2, 4, 6 and q = 0, 2, 4, 6 with

$q \leqslant k$. The energy level calculations employed the extended f-shell programs of Reid, in which the electronic levels were calculated by simultaneous diagonalization of various parameterized Hamiltonians for the 4f and 5d configurations of Ce^{3+} in YAG. A detailed description of the parameterized Hamiltonians and the calculations can be found in [25]. In the calculation of 4f energy levels, the value for the spin–orbit parameter, ζ (ff), was taken from that of Ce^{3+} in the LaF_3 crystal [26], while the values for the 4f crystal-field parameters, B_q^k (ff), were estimated from those of Pr^{3+} in YAG [27] by multiplying by the ratio of radial integrals $\langle r^k\rangle(Ce^{3+})/\langle r^k\rangle(Pr^{3+})$. These ratios were evaluated using a standard atomic computer program [28] with the values 1.089, 1.179, and 1.264 for $k = 2, 4, 6$, respectively. For the 5d configuration, the spin–orbit parameter, ζ (dd), was obtained by the atomic calculation on Ce^{3+} [28], and the five crystal-field parameters, B_0^2 (dd), B_2^2 (dd), B_0^4 (dd), B_2^4 (dd), and B_4^4 (dd), were derived from optimization with respect to the chosen experimental 5d levels of Ce^{3+} in YAG. In the optimization, the ratio B_2^2 (dd)/B_0^2 (dd) was fixed to the value for the 4f electron; hence a total of four parameters were freely varied within certain allowed ranges, with the signs being kept the same as the corresponding 4f parameters. The values were optimized by repeatedly calculating the 5d levels until the best agreement was obtained between the calculated and observed crystal-field levels. In addition, the Δ_E (fd) parameter, which accounts for the difference between the average energies of 5d and 4f configurations, was adjusted to obtain the best agreement between experiment and calculation. Due to the D_2 site symmetry of Ce^{3+} in YAG, there are three possible choices of the Z axis. Each has two possible orientations, which only affect the signs of the $q = \pm 2, \pm 4$ crystal-field parameters. In this work, the choice of the Z axis and its orientation is the same as in [27]. The band maxima, rather than the (undetermined) positions of zero phonon lines, were employed in the energy level calculations. This does not introduce fitting errors or crystal-field parameter changes, but serves to systematically displace all 5d-electron energies to higher energy, within the error of measurement of band positions.

Due to uncertainty in the assignment of experimental 5d levels, especially the level associated with 261 nm absorption (see later), three different scenarios for experimental 5d levels were explored for the determination of B_q^k (dd) parameters, mainly based upon the experimental studies of Tomiki *et al* [17]. In the first energy level set (I), the experimental level at $\sim$38 000 cm^{-1} (261 nm) was removed while the other four were kept unchanged. The second set (II) consists of only the lowest four experimental levels, and the third set (III) comprises all of the five experimental 5d levels of Tomiki *et al* [17]. The values for the 5d crystal-field parameter derived from the three calculations are collected in table 2, in which values for the other energy parameters described above are also included. In each of the three cases, the agreement between the calculated and experimental 5d energy level scheme is equally good, and these results are not listed, for clarity. However, as we shall see later in section 3.8, the choice of the first set of experimental 5d levels yields the best agreement between the calculated and experimental absorption intensities.

3.2. Calculation of $4f \rightarrow 5d$ *transition intensities*

Transitions from 4f to 5d levels are electric dipole allowed. The unpolarized transition intensities I_{if} of zero-phonon lines between the initial 4f levels $|f\Gamma_i\rangle$ and the final 5d levels $|d\Gamma_f\rangle$ may be expressed as

$$I_{if} \propto \bar{\nu}_{if} \sum_{q,\gamma_i,\gamma_f} |\langle f\Gamma_i\gamma_i|D_q^1|d\Gamma_f\gamma_f\rangle|^2 \tag{1}$$

where $\bar{\nu}_{if}$ is the transition wavenumber of zero-phonon lines, D_q^1 is the electric dipole operator, and the summation is over the polarization q ($q = 0, \pm 1$) and the components γ of the initial

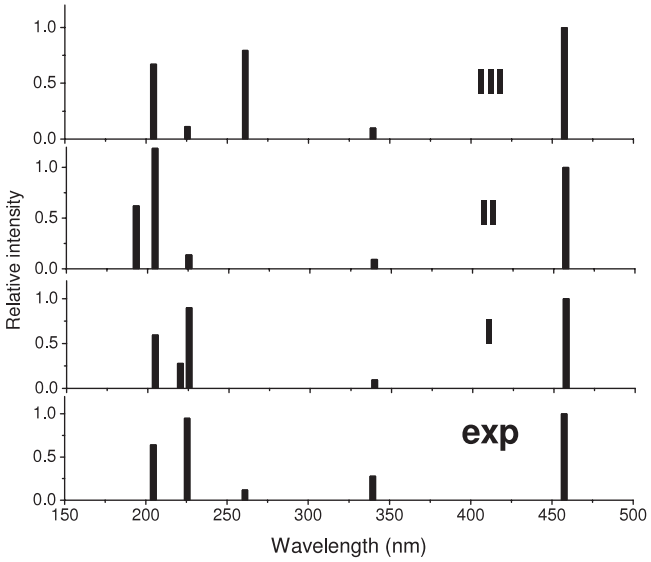

Figure 1. Schematic representations of relative intensities for 4f → 5d transitions from the ground 4f level to excited 5d levels of YAG:Ce^{3+}. The theoretical intensities in the upper three panels were calculated using the electronic wavefunctions derived by fitting three different sets of experimental 5d levels, as described in the text. The experimental values were taken from the absorption spectrum in [17].

Table 2. Energy parameters for the 4f and 5d configurations of Ce^{3+} in YAG. See the text for a detailed description of the parameters.

	4f				5d		
						cm^{-1}	
Parameter	cm^{-1}	Parameter	cm^{-1}	Parameter	I	II	III
ζ (ff)	647	B_0^6 (ff)	901	ζ (dd)	991	991	991
B_0^2 (ff)	−465	B_2^6 (ff)	307	B_0^2 (dd)	−6099	−1644	−8710
B_2^2 (ff)	−96	B_4^6 (ff)	2136	B_2^2 (dd)	−1259	−339	−1797
B_0^4 (ff)	−3739	B_6^6 (ff)	246	B_0^4 (dd)	−50 042	−58 960	−40 309
B_2^4 (ff)	−380	Δ (fd)	36 218	B_2^4 (dd)	−5374	−4197	−12 312
B_4^4 (ff)	1602			B_4^4 (dd)	19 626	18 569	18 164

and final levels. The expression for the electric dipole matrix elements in equation (1) may be found in [29]. These matrix elements were calculated using the pure electronic wavefunctions obtained in the aforementioned energy level calculations for 4f and 5d configurations. In the calculation, we made the approximation that the f → d transition intensity is proportional to that of the zero-phonon line.

The calculated relative f → d transition intensities from the ground 4f level to the excited 5d levels are listed in table 3, where the results for the three different cases (I, II, and III) as described above have all been included. A schematic representation of the results is given in figure 1. Following the presentation of the experimental data from this study, and a discussion of literature spectra, these results are further discussed in section 3.8.

Table 3. Calculated and experimental relative intensities of the f → d transitions from the ground 4f level to excited 5d levels.

5d absorption band (nm)	Relative absorption intensity from the ground 4f level			
Exp. [17, 18]	I	II	III	Exp. [17]
457.5	1	1	1	1.00
339.7	0.094	0.0935	0.098	0.28
261			0.795	0.12
225.4	0.899	0.138	0.113	0.95
204.6	0.594	1.191	0.671	0.642

3.3. X-ray diffraction

Figure 2 shows the room-temperature XRD patterns for YAG:Ce^{3+}-C-T and YAG: Ce^{3+}-P-T between $T = 800$ and 1100 °C. In each case, the samples are amorphous at 800 °C, but when the calcination temperature is 900–1100 °C the YAG phase is formed and there are no peaks from YAM or YAP. The average crystallite size D may be estimated by Scherrer's formula: $D = 0.89\lambda/(\beta \cos\theta)$, where λ denotes the x-ray radiation wavelength, 0.154 nm, and β stands for the observed full-width at half-maximum (FWHM) of a diffraction line located at $\theta°$, with the assumption that lattice strain broadening is negligible. The size of the particles increases by up to 50% with increasing calcination temperature from 900 to 1100 °C: for YAG:Ce^{3+}-C from 21 to 31 nm, and for YAG:Ce^{3+}-P from 25 to 31 nm, respectively.

3.4. FT-IR spectra

FT-IR spectra are sensitive tests for the identification of inorganic and organic impurities which are primarily located the surface of nanoparticles. Figure 3 shows the variations in the FT-IR spectra with temperature for the YAG:Ce^{3+}-C-T and YAG:Ce^{3+}-P-T samples. At a given temperature, the spectral features are similar for the two preparation methods. The spectra are broad for samples calcined at 800 °C, with bands due to OH stretching and bending vibrations at 3440–3480 and 1630 cm^{-1}; and other features at 1535, 1408 cm^{-1} which may be associated with carboxylate and nitrate modes. The IR spectra of YAG have been reported and assigned by Slack *et al*, and the 1100 °C spectra in figure 3 exhibit the same ten bands between 430 and 825 cm^{-1} as reported in [30]. These results give us confidence that the YAG:Ce^{3+} samples do not contain other phases.

3.5. XANES results

Literature x-ray near-edge absorption spectra (XANES) show that a clear identification and separation of Ce^{3+} and Ce^{4+} can be made for solid materials. For example, in [31], CeO_2 exhibits a doublet to high energy of the sharper, single peak of Ce^{3+} in $Ce(NO_3)_3{\cdot}6H_2O$. The Ce-L_3 x-ray absorption near-edge structure was examined for samples calcined at 800 and 1000 °C from the polymer-assisted sol–gel process. The results, figure 4, clearly show the coexistence of both Ce^{3+} and Ce^{4+} in the samples, with Ce^{4+} being dominant in the 800 °C sample.

3.6. Photoluminescence and excitation spectra between 250 and 600 nm

The spectra for samples prepared by the co-precipitation method and the polymer-assisted sol–gel process are very similar for Xe-lamp excitation at room temperature, figure 5(a), and are the same as reported in the literature; see, e.g. [32]. The emission band peaks at 530 nm for samples calcined at 900 °C and above. The lowest-energy excitation band peaks at 467 nm so that the zero-phonon line of the transition from the electronic ground state to the lowest 5d level

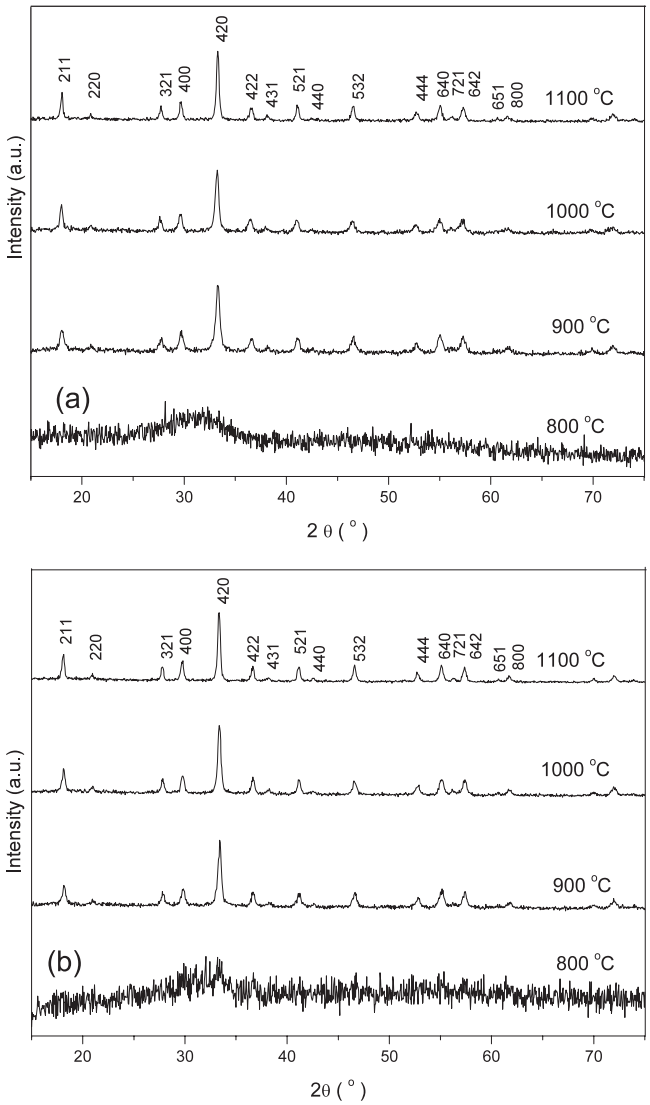

Figure 2. Room-temperature XRD patterns for (a) YAG:Ce^{3+}-C-T and (b) YAG:Ce^{3+}-P-T between $T = 800$ and 1100 °C.

is estimated to be at 497 nm (20 140 cm^{-1}). Since the vibrational displacement between 497 and 530 nm is ∼1270 cm^{-1}, we can also infer that the maximum intensity of the emission band corresponds to the $v'' = 2$ member of a vibrational progression, since 1270 ∼ $(v'')h\nu$ and the maximum energy of the Y–O stretch is ∼830 cm^{-1}. However, this may not be the case since there are other electronic transitions to the crystal field levels of $^2F_{5/2}$.

The maximum emission wavelength is situated at 530 nm when the calcination temperature is between 900 and 1100 °C, as also found by Fu [14]. Xia *et al* have reported a blue shift (∼3 nm) of the emission band within this temperature range [8], and attributed this to the decrease in lattice constant with increasing temperature. Actually, such a decrease in lattice constant (and smaller Ce–O distance) should produce a red shift, not a blue shift. It is well known that a considerable red shift of the emission band results for $Ln_3Al_5O_{12}$:Ce^{3+} (Ln = Y,

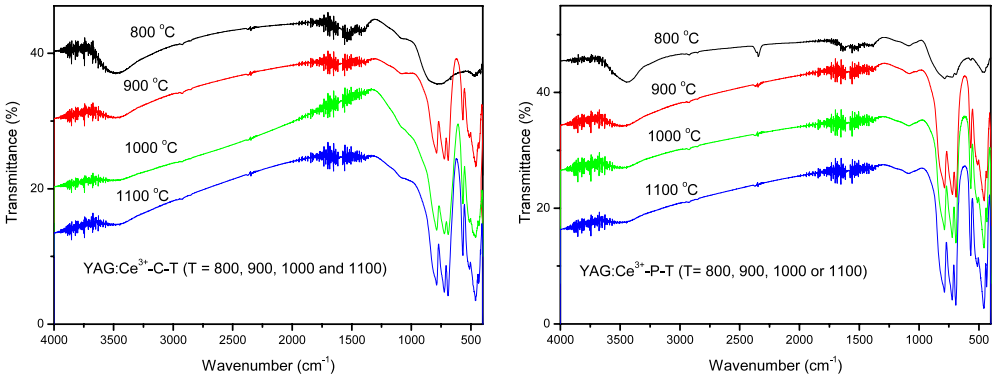

Figure 3. Room-temperature FT-IR spectra for (a) YAG:Ce^{3+}-C-T and (b) YAG:Ce^{3+}-P-T between $T = 800$ and 1100 °C.

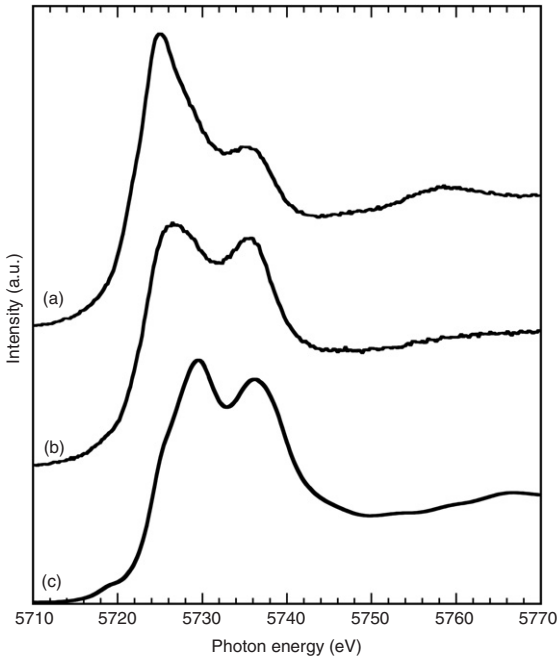

Figure 4. Ce-L_3 x-ray absorption near-edge structure in YAG:Ce^{3+}-P-T for (a) $T = 1000$ °C and (b) 800 °C in comparison to (c) CeO_2.

Lu) when Ln^{3+} at a dodecahedral site is replaced by a larger tripositive cation [6, 22], e.g. a ∼30 nm shift [15] for the substitution of Y^{3+} (VIII) (101.9 pm [33]) by Gd^{3+} (VIII) (105.3 pm). This has been attributed to the larger crystalline field experienced by Ce^{3+}, resulting from a decrease in Ce–O distance, leading to an increased d-orbital splitting. Furthermore, the greater $4f^1$ crystal-field splitting is expected to extend the emission band to longer wavelengths. In the literature, the emission red shift upon increasing Ce^{3+} concentration in YAG:Ce^{3+} has been attributed to self-absorption, changes in unit cell lattice parameters, inhomogeneous broadening effects, the production of new Ce^{3+} sites and/or Ce^{3+}–Ce^{3+} interactions [1, 4, 8, 19, 22], although others have disputed whether such an effect actually occurs [34].

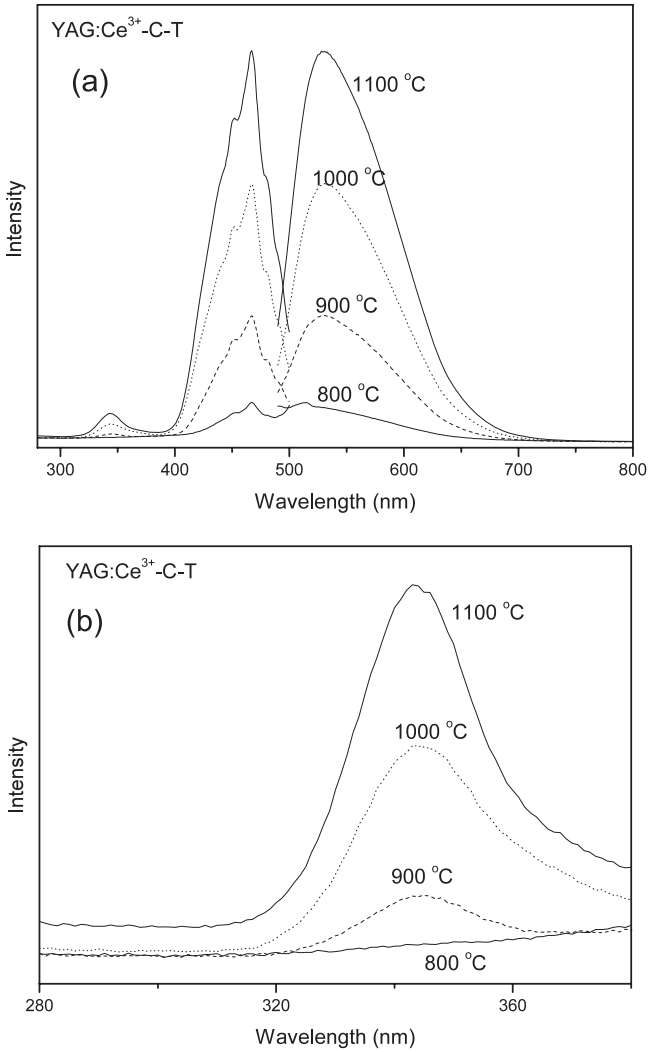

Figure 5. Xe-lamp emission spectra and excitation spectra (monitoring the emission at 530 nm) of YAG:Ce^{3+}-C-*T* for calcination temperatures between 800 and 1100 °C: (a) emission and excitation spectra between 280 and 800 nm; (b) excitation spectrum between 260 and 380 nm. The shoulders in the excitation spectrum between 437 and 491 nm are due to Xe-lamp lines. The spectral resolution was 2 nm.

Zhou *et al* [35] reported a blue shift of 2 nm for the transitions to $5d_1$, $5d_2$ in the excitation spectra of the room-temperature emission of nanocrystalline YAG:Ce^{3+}, compared with the bulk material. These authors also noted that the unit cell parameters of the nanocrystals were smaller than that for the bulk crystal. A blue shift is also evident in the excitation spectrum of Isobe [36], where the excitation spectrum of the nanocrystal exhibits broader spectral features than the bulk crystal. Li *et al* [7] and Jia *et al* [37] have also reported blue shifts. However, it is evident that the shift is small compared with the FWHM of about 50 nm for the emission band width. As mentioned above, a decrease in lattice parameter is expected to give rise to a red shift for the lower d-electron crystal-field levels. Also, such factors as the ambient atmosphere,

type of flux, etc in the preparation method of YAG:Ce^{3+} are known to produce band shifts of a larger magnitude even for bulk crystals [15].

Under constant excitation intensity, the emission intensity increases by an order of magnitude when the calcination temperature of the YAG:Ce^{3+} sample is increased from 800 to 1100 °C, figure 5(a). A similar behaviour was observed in the sol–gel combustion synthesis of YAG:Ce^{3+} using citric acid as fuel, and was attributed to the improved crystalline and homogeneous distribution of Ce^{3+} ions at higher temperature [8]. The emission intensity as a function of excitation wavelength for the YAG:Ce^{3+}-C-1100 sample is much greater for excitation into the peak of the first 4f–5d absorption band at 467 nm than into the peak of the second band at 343 nm. This second excitation band shows an interesting behaviour when the calcination temperature increases, figure 5(b). It is not apparent in the excitation spectrum of the YAG:Ce^{3+}-C-800 sample and steadily increases in intensity with increasing temperature. Thus a strongly absorbing centre is present in the YAG:Ce^{3+}-C-800 sample which is steadily removed on increasing the calcination temperature. With reference to the XANES results, one candidate is Ce^{4+} which has a band gap of 3.51 eV (353 nm) in CeO_2 and exhibits a broad absorption band to high energy of ∼500 nm [38]. Thus, a further reason why the intensity of luminescence increases with calcination temperature under ultraviolet excitation is because the concentration of Ce^{4+} absorbing centres (acting as killer sites) decreases.

The 10 K emission spectra of YAG:Ce^{3+} samples prepared by both methods were recorded under 460 nm laser excitation in the region below 21 300 cm^{-1}, and the yellow emission exhibited a structured band due to the transitions to the $^2F_{5/2,\,7/2}$ multiplet terms.

3.7. Synchrotron radiation excited emission and excitation spectra

At room temperature and at 10 K, the vacuum ultraviolet excitation spectrum of the emission at 522 nm of a sample of YAG:Ce^{3+}-P-1100 shows a sharp increase in intensity at 184 nm (54 350 cm^{-1}) which continues to increase until about 155 nm (64 520 cm^{-1}). The structure in this region is very similar to that in the excitation spectrum of undoped YAG and corresponds to the band-gap excitation of YAG so that host–guest ion energy transfer occurs in YAG:Ce^{3+}. The intensity of the excitation peak at 225 nm (44 440 cm^{-1}) is much weaker and no further bands are observed up to our observation limit at 300 nm. The corresponding results for a sample prepared by the co-precipitation method are shown in figure 6(a), and a slight low-temperature shift to high energy is apparent for the band centred at 229 nm at room temperature. Again, no feature is evident between 260 and 270 nm (38 460–37 040 cm^{-1}). The corresponding emission spectra under excitation into the Ce^{3+} absorption band at 225 nm for the co-precipitation and polymer-assisted samples are shown in figures 6(b) and (c), respectively. Besides the intense band centred at 522 nm, a long-wavelength shoulder is more clearly resolved at 10 K at 585 ± 6 nm which corresponds to the partially resolved transition to the upper $^2F_{7/2}$ multiplet term. The 225 nm-excited spectrum of the polymer-assisted sample (figure 6(c)) exhibits two impurity emission bands at 377, 420 nm which are not present in the corresponding spectrum of the co-precipitation sample (figure 6(b)). The spike at 687 nm in figure 6(c) corresponds to Cr^{3+} R-line emission, and that near 670 nm in figures 6(b) and (c) to Mn^{4+} emission.

Under band-gap excitation at 178 nm, an additional emission band is observed which blue shifts and sharpens to be located near 320 nm on cooling to 10 K (figures 6(b) and (c)). The excitation spectrum of this emission (figure 6(a)) does not exhibit Ce^{3+} absorption bands, but only shows the host band-gap features. Owen *et al* [39] performed excited-state absorption (ESA) experiments upon YAG:Ce^{3+} and proposed that a transition from the lowest 5d level of Ce^{3+} to the conduction band occurred. This ESA transition would be at about 55 550–20 140 ∼ 35 400 cm^{-1} (282 nm) so that an assignment of the corresponding emission band

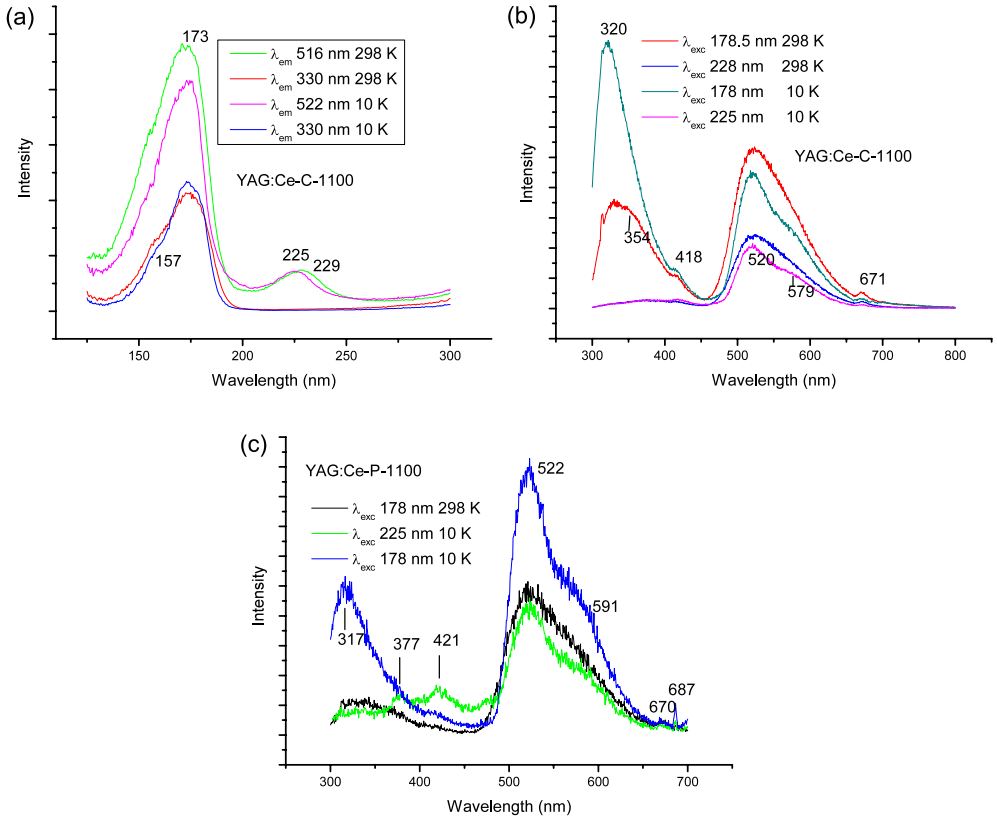

Figure 6. Synchrotron radiation excitation and emission spectra of YAG:Ce^{3+}-C-1100 and YAG:Ce^{3+}-P-1100 at room temperature and 10 K: (a) for the excitation spectra of YAG:Ce-C-1100; (b) for the emission spectra of YAG:Ce-C-1100; (c) for the emission spectra of YAG:Ce-P-1100.

with a maximum at 320 nm to the recombination process $Ce^{4+} + e \rightarrow Ce^{3+}$ is possible. This type of process is distinct from electron–hole recombination processes (i.e. self-trapped exciton emission) which, for example, have been discussed for isovalent ions doped into YAG [40] or anti-site defects (for example, Y^{3+}_{Al}, where Y^{3+} occupies the Al^{3+} site [41–44]). However, other assignments of this emission band are possible, as discussed now.

It is well known that the large unit cell of YAG is susceptible to many defect sites and impurities, especially when high-temperature growth produces lattice strain. The paper of Zych *et al* discusses the role of more than ten traps as shown in the thermoluminescence of YAG:Ce^{3+} [45]. From the optical spectra of rare earth garnets, spectral features have been associated with four types of activator ion defects [46]. In the case of YAG:Ce^{3+} additional defect sites arise from Y^{3+}_{Al} anti-site defects, the presence of other rare earth ion impurities, or heterovalent impurity species. For the latter, M^{2+} is predicted to occupy 8-coordinated rare earth sites and produce oxygen vacancies; whereas M^{4+} dopants reside on both Al^{3+} and rare earth sites and are compensated by rare earth vacancies [31]. Finally, it is noted that the ionic radius of the dopant ion Ce^{3+} (VIII), 114.3 pm, [33] is not too different from that of Y^{3+} (VIII), 101.9 nm, but very different from Al^{3+} (VI), 53.5 pm, and Al^{3+} (IV), 39 pm, so at low concentrations and low synthesis temperatures it substitutes solely for Y^{3+}.

In view of the many possible interpretations, some different explanations have previously been given for the ultraviolet luminescence bands of YAG:Ce^{3+}, and the locations of these

bands are not always the same as in the present study. Note that YAG:Pr^{3+} has a broad ultraviolet emission band with sub-peaks at 317, 340, 369 nm [47]. However, the anomalous emission bands observed in our spectra do not correspond to emission from Pr^{3+} impurity because the weak, sharp bands expected to lower energy from $4f^2$–$4f^2$ emission are not present. The emission band observed at 300 nm in YAG:Ce^{3+} single crystals under x-ray excitation was not apparent in ceramic materials and was assigned to an exciton localized around the Y^{3+}_{Al} anti-site defect or to a recombination luminescence arising around this defect [48]. In fact, the energy of this emission band was found to be rather insensitive to the nature of other trivalent ions occupying the Y^{3+} (VIII) site, but emission bands at similar energy were observed for YAG crystals where other trivalent ions occupy the Al^{3+} (VI) site [44]. In undoped YAG the broad room-temperature emission at 314 nm shifts to 258 nm on cooling to 85 K [21].

Finally, emission from the second excited 5d level to the electronic ground state in YAG:Ce^{3+} has been postulated by Blasse and Bril since emission bands were observed at 27 800 and 29 200 cm^{-1} (360, 342 nm) under 254 nm excitation at room temperature [19]. In another study, bands were observed at 25 650 and 27 580 cm^{-1} (390, 363 nm) at 4.2 K [43]. This excited 5d level ($5d_2$) lies below the conduction band [39] and is ∼7500 cm^{-1} above $5d_1$. In the first case, the corresponding excitation spectrum peak maximum was at 29 400 cm^{-1} (340 nm), so the Stokes shift would only be 200 cm^{-1}, and this is considered improbable. The assignment is plausible in the second case at low temperature, where the Stokes shift is 2904 cm^{-1} and the separation between the two emission bands (1936 cm^{-1}) is exactly the same as between the visible emission bands reported by these authors.

3.8. Energy level assignments for YAG:Ce^{3+}

We now return to the problematic 5d-electron energy level assignments for Ce^{3+} as illustrated in table 1. Considering the various literature assignments for the absorption and excitation spectra of YAG:Ce^{3+} it is noted that the 255–270 nm absorption band exists in undoped YAG [49, 50] and in the excitation spectrum of the 300 nm defect emission [49]. This band is clearly absent in many of the reported absorption spectra of YAG:Ce^{3+} [1, 4, 5, 20, 32, 48] as well as from the excitation spectrum of Ce^{3+} emission reported in this work and in other studies [45, 50, 51]. The 261 nm feature was fitted as a Gaussian by Tomiki *et al* in figure 3 of [17], but the intensity in that spectral region is very weak and its existence is questionable. Thus, in view of its absence in the ultraviolet spectra of YAG:Ce^{3+} recorded in other literature, we do not assign it to a transition of Ce^{3+}. The intensity calculation for scenario III which follows the energy level assignments by Tomiki *et al* [17] predicts an intensity profile in figure 1 which shows that the 261 nm band should be stronger than the higher-energy features, and this is clearly not so. On discarding this band, the scenarios I and II in figure 1 are clearly distinguished by the fact that the 225 nm band is predicted to be stronger (I) or weaker (II) than the 205 nm band, and experiment then indicates scenario I is applicable. We therefore propose that the $5d_4$-electron level lies between the $5d_3$ and $5d_5$, so that the weak transition to it is masked by the two stronger, adjacent transitions. The assigned energy value to $5d_4$ in figure 1 is nominal (since it is not experimentally determined), and its adjustment does not noticeably influence the calculated intensities.

4. Conclusions

In this study YAG:Ce^{3+} has been synthesized as nanoparticles by two low-temperature routes and characterized by IR spectroscopy, XRD and XANES. The XRD patterns showed that when the calcination temperature is 900 °C or higher, a pure YAG phase was obtained for both of

the two methods. The more sensitive test of purity by FT-IR spectra indicated the absence of impurities when the materials were calcined at 1000 or 1100 °C and the YAG phase was formed. The room-temperature Xe-lamp photoluminescence excitation spectra show that there are two Ce^{3+} excitation bands located at around 342 and 467 nm in the region of 300–500 nm due to the transitions to the crystal-field split 5d electronic state of Ce^{3+}. The synchrotron radiation excitation spectra of the yellow emission band show a further band attributed to Ce^{3+} near 225 nm, as well as the YAG band-gap excitation. The origin of the emission band at 320 nm has been discussed, and it is not due to Ce^{3+}. Evidence is presented that the Ce^{4+} ions present in the samples calcined at the lower temperature of 900 °C are at least in part responsible for reduced luminescence intensity.

Fitting the 5d energy levels of Ce^{3+} under certain different scenarios provides wavefunctions which were employed to calculate 4f–5d transition intensities. The calculated relative intensities for scenario (I) (where the assignment of a band at 261 nm to Ce^{3+} is rejected) agree well with experiments, whereas the other two scenarios do not agree. It is therefore proposed that the transition 4f–$5d_4$ lies between the two much stronger absorptions (204 and 225 nm) and is thus not observed. The scenarios I–III are associated with rather different crystal-field parameters for the d electrons (table 2), with II and III usually exhibiting the extreme values.

Acknowledgments

This work is supported by the City University Strategic Research Grant 7001837. We thank the National Synchrotron Radiation Research Centre, Taiwan, for granting beam time under Proposal 2005-3-085-3, and SPring8, Japan for Proposal No. 2006B1370. Experimental Ce-L_3 XANES work at SPring8 by T Sakai, F Oba and I Tanaka of Kyoto University, Japan is gratefully acknowledged.

References

[1] Yanagida T, Takahashi H, Ito T, Kasama D, Enoto T, Sato M, Hirakuri S, Kokobun M, Makishima K, Yanagitani T, Yagi H, Shigeta T and Ito T 2005 *IEEE Trans. Nucl. Sci.* **52** 1836
[2] Ludziejewski T, Moszyński M, Kapusta M, Wolski D, Klamra W and Moszyńska K 1997 *Nucl. Instrum. Methods Phys. Res.* A **398** 287
[3] Mita Y, Kobayashi T, Miyamoto Y, Ishii O and Sawanobori N 2004 *Phys. Status Solidi* b **241** 2672
[4] Haranath D, Chander H, Sharma P and Singh S 2006 *Appl. Phys. Lett.* **89** 173118
[5] Zhao G J, Zeng X H, Xu J, Zhou S M and Zhou Y Z 2003 *Phys. Status Solidi* a **199** 355
[6] Holloway W W and Kestigian M 1969 *J. Opt. Soc. Am.* **59** 60
[7] Li Q, Gao L and Yan D S 2000 *Mater. Chem. Phys.* **64** 41
[8] Xia G, Zhou S, Zhang J and Xu J 2005 *J. Cryst. Growth* **279** 357
[9] Veith M, Mathur S, Kareiva A, Jilavi M, Zimmer M and Huch V 1999 *J. Mater. Chem.* **9** 3069
[10] Chiang C C, Tsai M S, Hsiao C S and Hon M H 2006 *J. Alloys Compounds* **416** 265
[11] Kasuya R, Isobe T and Kuma H 2006 *J. Alloys Compounds* **408–412** 820
[12] Kasuya R, Isobe T, Kuma H and Katano J 2005 *J. Phys. Chem.* B **109** 22126
[13] De la Rosa E, Diaz-Torres L A, Salas P, Arredondo A, Montoya J A, Angeles C and Rodriguez R A 2005 *Opt. Mater.* **27** 1793
[14] Fu Y-P 2006 *J. Alloys Compounds* **414** 181
[15] Pan Y, Wu M and Su Q 2004 *J. Phys. Chem. Solids* **65** 845
[16] Miniscalco W J, Pellegrino J M and Yen W M 1979 *J. Appl. Phys.* **49** 6109
[17] Tomiki T, Kohatsu T, Shimabukuro H and Ganaha Y 1992 *J. Phys. Soc. Japan* **61** 2382
[18] Reyher H-J, Hausfeld N, Pape M, Baur J and Schneider J 1999 *Solid State Commun.* **110** 345
[19] Blasse G and Bril A 1967 *J. Chem. Phys.* **47** 5139
[20] Dong Y, Zhou G, Xu J, Zhao G, Su F, Su L, Zhang G, Zhang D, Li H and Si J L 2006 *Mater. Res. Bull.* **41** 1959

[21] Babin V, Blazek K, Krasnikov A, Nejezchleb K, Nikl M, Savikhina T and Zazubovich S 2005 *Phys. Status Solidi* c **2** 97
[22] Setlur A A and Srivastava A M 2006 *Opt. Mater.* (doi:10:1016/j.optimat.2006.08.010)
[23] Lu H-C, Chen H-K, Tseng T-Y, Kuo W-L, Alam M S and Cheng B-M 2005 *J. Electron Spectrosc. Relat. Phenom.* **144–147C** 983
[24] Euler F and Bruce J A 1965 *Acta Crystallogr.* **19** 971
[25] Reid M F, van Pieterson L, Wegh R T and Meijerink A 2000 *Phys. Rev.* B **62** 14744
[26] Carnall W T, Goodman G L, Rajnak K and Rana R S 1989 *J. Chem. Phys.* **90** 3443
[27] Moune O K, Rabinovitch Y, Tétard D, Pham-Thi M, Lallier E and Faucher M D 2002 *Eur. Phys. J.* D **19** 275
[28] Cowan R D 1981 *The Theory of Atomic Structure and Spectra* (Berkeley, CA: University of California)
[29] Ning L, Jiang Y, Xia S and Tanner P A 2003 *J. Phys.: Condens. Matter* **15** 7337
[30] Slack G A, Oliver D W, Chrenko R M and Roberts S 1969 *Phys. Rev.* **177** 1308
[31] Wu Z, Benfield R E, Guo L, Li H, Yang Q, Grandjean D, Li Q and Zhu H 2001 *J. Phys.: Condens. Matter* **13** 5269
[32] Jacobs R R, Krupke W F and Weber M J 1978 *Appl. Phys. Lett.* **33** 410
[33] http://abulafia.mt.ic.ac.uk/shannon/ptable.php
[34] Yan M F, Huo T C D and Ling H C 1987 *J. Electrochem. Soc.* **134** 493
[35] Zhou S, Fu Z, Zhang J and Zhang S 2006 *J. Lumin.* **118** 179
[36] Isobe T 2006 *Phys. Status Solidi* a **203** 2686
[37] Jia D, Wang Y, Guo X, Li K, Zou Y K and Jia W 2007 *J. Electrochem. Soc.* **154** J1
[38] Zhang D-E, Zhang X-J, Ni X-M, Song J-M and Zheng H-G 2006 *Chem. Phys. Lett.* **430** 326
[39] Owen J F, Dorain P B and Kobayashi T 1981 *J. Appl. Phys.* **52** 1216
[40] Mürk V and Yaroshevich N 1995 *J. Phys.: Condens. Matter* **7** 5857
[41] Stanek C R, McClellan K J, Levy M R and Grimes R W 2006 *Phys. Status Solidi* b **243** R75
[42] Nikl M, Mihokova E, Pejchal J, Vedda A, Zorenko Y and Nejezchleb K 2005 *Phys. Status Solidi* b **242** R119
[43] Blazek K, Krasnikov A, Nejezchleb K, Nikl M, Savikhina T and Zazubovich S 2004 *Phys. Status Solidi* b **241** 1134
[44] Zorenko Y 2005 *Phys. Status Solidi* c **2** 375
[45] Zych E, Brecher C and Glodo J 2000 *J. Phys.: Condens. Matter* **12** 1947
[46] Lupei A, Lupei V and Osiac E 1998 *J. Phys.: Condens. Matter* **10** 9701
[47] Meltzer R S, Zheng H, Wang J W, Yen W M and Grinberg M 2005 *Phys. Status Solidi* c **2** 284
[48] Mihokova E, Nikl M, Mares J A, Beitlerova A, Vedda A, Nejezchleb K, Blazek K and D'Ambrosio C 2006 *J. Lumin.* (doi:10:1016/j.jlumin.2006.05.004)
[49] Wong C M, Rotman S R and Warde C 1984 *Appl. Phys. Lett.* **44** 1038
[50] Dong Y, Zhou G, Xu J, Zhao G, Su F, Su L, Li H, Si J-L, Qian X, Li X and Shen J 2006 *J. Cryst. Growth* **286** 476
[51] Wang Z, Xu M, Zhang W and Yin M 2007 *J. Lumin.* **122/123** 427